JACS
JOURNAL OF THE AMERICAN CHEMICAL SOCIETY
Article
pubs.acs.org/JACS

Dissociation of the K-Ras4B/PDEδ Complex upon Contact with Lipid Membranes: Membrane Delivery Instead of Extraction

Katrin Weise,[†] Shobhna Kapoor,[†] Alexander Werkmüller,[†] Simone Möbitz,[†] Gunther Zimmermann,[‡,§] Gemma Triola,[‡,§] Herbert Waldmann,[‡,§] and Roland Winter*[,†]

[†]Physical Chemistry I - Biophysical Chemistry, Faculty of Chemistry, TU Dortmund University, Otto-Hahn-Strasse 6, D-44227 Dortmund, Germany

[‡]Department of Chemical Biology, Max Planck Institute of Molecular Physiology, Otto-Hahn-Strasse 11, D-44227 Dortmund, Germany

[§]Chemical Biology, Faculty of Chemistry, TU Dortmund University, Otto-Hahn-Strasse 6, D-44227 Dortmund, Germany

Supporting Information

ABSTRACT: K-Ras4B is a small GTPase whose selective membrane localization and clustering into microdomains are mediated by its polybasic farnesylated C-terminus. The importance of the subcellular distribution for the signaling activity of K-Ras4B became apparent from recent *in vivo* studies, showing that the delta subunit of cGMP phosphodiesterase (PDEδ), which possesses a hydrophobic prenyl-binding pocket, is able to function as a potential binding partner for farnesylated proteins, thereby leading to a modulation of the spatiotemporal organization of K-Ras. Even though PDEδ has been suggested to serve as a cytosolic carrier for Ras, the functional transport mechanism still remains largely elusive. In this study, the effect of PDEδ on the interaction of GDP- and GTP-loaded K-Ras4B with neutral and anionic model biomembranes has been investigated by a combination of different spectroscopic and imaging techniques. The results show that PDEδ is not able to extract K-Ras4B from membranes. Rather, the K-Ras4B/PDEδ complex formed in bulk solution turned out to be unstable in the presence of heterogeneous membranes, resulting in a release of farnesylated K-Ras4B upon membrane contact. With the additional observation of enhanced membrane affinity for the K-Ras4B/PDEδ complex, a molecular mechanism for the PDEδ–K-Ras4B-membrane interaction could be proposed. This includes an effective delivery of PDEδ-solubilized K-Ras4B to the plasma membrane, probably through cytoplasmic diffusion, the dissociation of the K-Ras4B/PDEδ complex upon plasma membrane contact, and finally the membrane binding of released farnesylated K-Ras4B that leads to K-Ras4B-enriched microdomain formation.

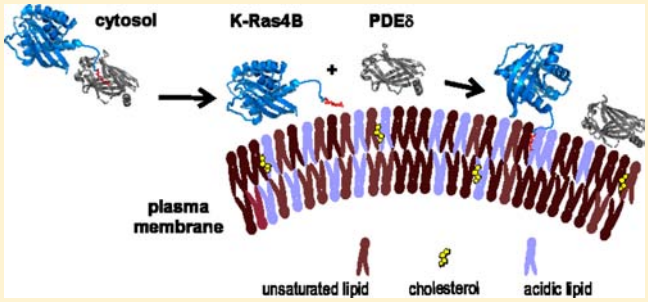

INTRODUCTION

K-Ras4B plays a critical role in human cancer cell biology, with mutationally activated K-Ras frequently identified in pancreatic adenocarcinomas, colon adenomas, and lung carcinomas.[1−3] The aberrant control of signaling pathways in tumor cells by constitutively active Ras leads—among others—to uncontrolled cell proliferation, differentiation, and death. K-Ras4B is a member of the Ras family of small GTP-binding proteins that act as molecular switches between a GDP-bound inactive and GTP-bound active state.[4−6] Signal transmission from cell surface receptors to intracellular signaling cascades by K-Ras4B critically depends on the subcellular distribution and correct localization of K-Ras4B. The targeting of K-Ras4B to the negatively charged cytosolic leaflet of the plasma membrane is directed by a specific membrane-interacting and -targeting signal that consists of a C-terminal polybasic stretch of six contiguous lysines in a total of eight, which directly precedes the terminal farnesylated and carboxymethylated cysteine residue (Figure 1).[5,7−10] Electrostatic interactions are thought to drive the intracellular transport of K-Ras4B between subcellular compartments, with the polybasic domain acting as a probe for the negative surface potential of the membrane.[11,12] In a recent study, we were able to show that K-Ras4B is preferentially localized in liquid-disordered lipid domains of heterogeneous membranes and forms new protein-enriched fluid domains that probably recruit multivalent acidic lipids by an effective, electrostatic lipid-sorting mechanism, thus enabling K-Ras4B-specific interactions from separate membrane microdomains.[13] However, in the spatial cycling of K-Ras4B between the plasma membrane and internal localizations such as the endoplasmic reticulum, late endosomes, or mitochondria, the exact transport mechanism of K-Ras4B to the plasma membrane remains elusive.[14−16]

Received: February 28, 2012
Published: June 21, 2012

dx.doi.org/10.1021/ja305518h | J. Am. Chem. Soc. 2012, 134, 11503−11510

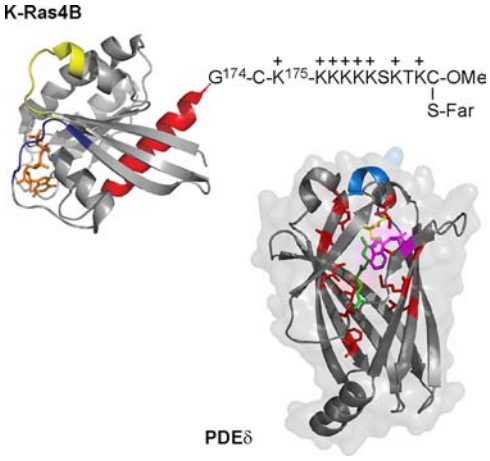

Figure 1. Schematic representation of the structures of K-Ras4B and PDEδ (PDB codes: 3GFT and 3T5G, respectively; images generated with PyMOL). The synthesized, lipidated K-Ras4B peptide was ligated to a truncated K-Ras4B protein expressed in *E. coli* to yield the *S*-farnesylated K-Ras4B protein bearing an additional cysteine between Gly^{174} and Lys^{175}.[20] The switch I region of the G-domain (aa 32−38) is shown in blue, the switch II region (aa 59−67) in yellow, and the helix α5 (aa 151−166) is colored in red. For PDEδ the structure was adopted from the PDB to highlight the residues forming the hydrophobic binding pocket (M20, L22, L38, I53, L63, I129, F133, L147, Y149; red), the flexible loop (aa 111−117; blue), and the tryptophan residue W32 (magenta). The farnesylated cysteine of a small GTPase that is incorporated in the hydrophobic binding pocket of PDEδ in the complex, is shown in green (Far) and yellow (Cys).[21]

The delta subunit of retinal rod cGMP phosphodiesterase 6 (PDEδ) has been proposed to function as a cytoplasmic prenyl binding factor and accordingly is supposed to assist in the intracellular trafficking and proper signaling of Ras.[17,18] Previous studies have shown that PDEδ is able to bind and solubilize several proteins from the Ras superfamily, such as Ras and Rheb.[17−21] Hence, PDEδ would allow Ras proteins to shuttle between cellular membranes by shielding the hydrophobic anchor (particularly farnesyl)[19,20] from the cytosol, thus facilitating intracellular Ras diffusion. Recent work by Wittinghofer et al. revealed that binding of prenylated small G-proteins to PDEδ occurs mainly through a deep insertion of the farnesylated C-terminus into the hydrophobic pocket of PDEδ (Figure 1).[17,21] No interaction of PDEδ with the G-domain's switch regions could be detected, implying a nucleotide-independent binding to PDEδ.[18,21] A PDEδ-mediated extraction of membrane-anchored Ras proteins from cellular membranes was also proposed,[18,22] but no direct molecular-level evidence for such a mechanism could be obtained so far.

Until now, most of the studies on the function of PDEδ have been carried out either in bulk solution, i.e., in the absence of membranes,[19−21,23] or in cellular systems.[17−19,21,22,24,25] To gain mechanistic insight into the interaction of K-Ras4B and PDEδ in the presence of membranes with molecular resolution, a combination of different biophysical techniques was used in the present study. The interaction of semisynthetic fully functional lipidated, GDP- and GTP-loaded (GppNHp-bound state as a nonhydrolyzable GTP analogue) K-Ras4B[20] as well as PDEδ and the K-Ras4B/PDEδ complex with neutral and anionic model biomembranes has been investigated. As heterogeneous model membrane systems, two well-established neutral and anionic lipid raft mixtures that consist of DOPC/DPPC/Chol, 25:50:25 (molar ratio) and DOPC/DOPG/DPPC/DPPG/Chol, 20:5:45:5:25 (molar ratio), respectively, were used.[26,27] From the combined results of this study, a molecular mechanism of the PDEδ−K-Ras4B-membrane interaction could be proposed. This involves an effective delivery of PDEδ-solubilized K-Ras4B to the plasma membrane, the dissociation of the K-Ras4B/PDEδ complex upon plasma membrane contact, and finally the membrane binding of released farnesylated K-Ras4B that leads to K-Ras4B-enriched microdomain formation.

RESULTS

Membrane Binding Kinetics of K-Ras4B and PDEδ. Surface plasmon resonance (SPR) allows the detection of binding and dissociation kinetics of proteins to and from a membrane surface in real-time by measuring changes in the resonance angle.[28] The resulting sensorgram comprises a plot of the SPR signal in resonance units (1 RU = 1 pg mm^{-2}, i.e., surface coverage with protein in terms of mass protein/mm^2 surface area) against time.[29,30] The lipid bilayer is immobilized on a lipophilic modified dextran matrix of an L1 sensor chip,[31,32] and the protein solution is injected across the surface. Since it has been shown that lipidated Ras proteins relocate and cluster on lipid surfaces after membrane insertion,[13,33,34] a two-step process was assumed for the analysis of the association and dissociation phase of the protein−membrane interaction process (cf. Supporting Information [SI]).[32] From the SPR sensorgrams, the membrane interaction of the proteins can be quantified by determining three representative parameters: the initial slope of the association phase that allows a comparison of the incipient affinities of the proteins to the lipid membranes, the average dissociation rate constant, $\overline{k}_{diss}$, which quantifies the overall dissociation rate of the protein from the lipid membrane, and the relative amount of quasi-irreversibly bound protein at the end of each dissociation phase that reflects the ability of the protein to stably insert into the lipid membrane (cf. SI Text and Tables S1 and S2).

To directly test the hypothesis that PDEδ is able to extract K-Ras4B from membranes,[18] SPR experiments were carried out that included the binding of GDP- and GTP-loaded K-Ras4B (2 μM) to neutral or anionic lipid raft membranes and subsequent injection of PDEδ (3.4 μM). The sensorgrams show that, independent of Ras nucleotide loading and membrane composition, PDEδ is not able to extract K-Ras4B from membranes since the amount of membrane-bound K-Ras4B and hence the SPR signal is not reduced by the addition of PDEδ (Figures 2a and S1a of SI). Instead, the addition of PDEδ to membrane-bound K-Ras4B results in an increase in the response measured, indicating that PDEδ itself binds to the membrane even in the presence of membrane-bound K-Ras4B and that the latter is not released in the presence of PDEδ. Changing the PDEδ-containing solution to buffer also does not reveal an enhanced dissociation of the protein from the membrane. Thus, in subsequent experiments, K-Ras4B and PDEδ were premixed in bulk solution to allow complex formation. The analysis of the corresponding sensorgrams reveals that PDEδ accelerates the binding of K-Ras4B in particular to anionic lipid raft membranes, indicating an increased membrane affinity in the complexed state for GDP- and GTP-loaded K-Ras4B (Figure 2b). Interestingly, PDEδ itself exhibits a strong affinity to both anionic and neutral raft membranes as implied by the relatively large initial slopes of the SPR sensorgrams. The influence of PDEδ on the association

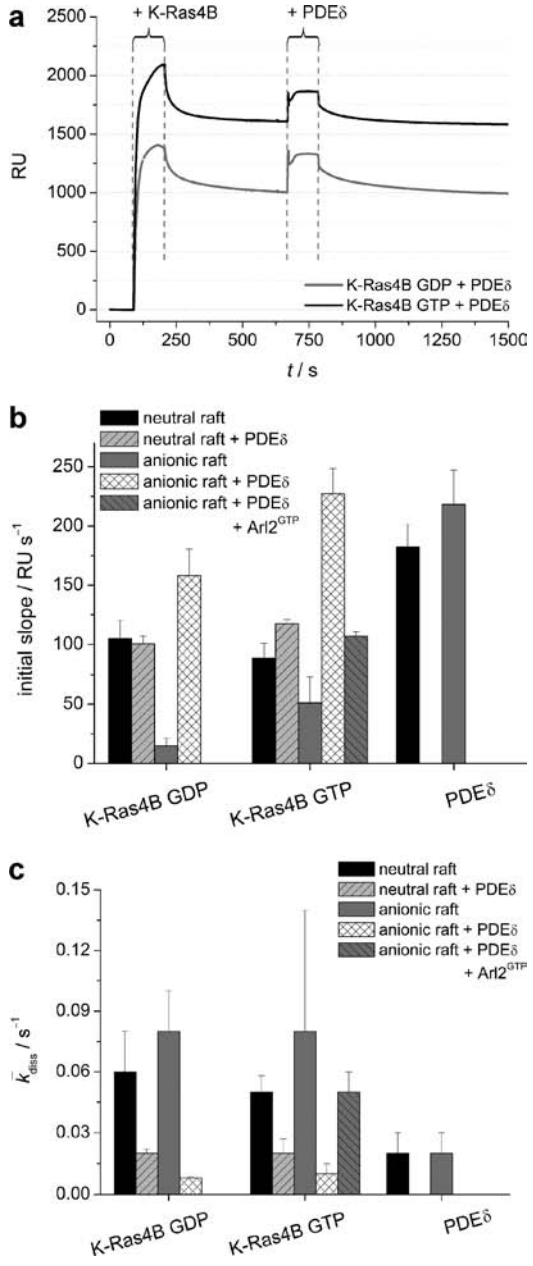

Figure 2. (a) SPR sensorgrams of the binding of GDP- and GTP-loaded K-Ras4B (c = 2 μM) to anionic raft membranes and subsequent addition of PDEδ (c = 3.4 μM). Panels b and c show the summarized SPR data for the initial association process (b) and the average dissociation rate constant $\bar{k}_{diss}$ (c) for GDP- and GTP-loaded K-Ras4B as well as PDEδ and the K-Ras4B/PDEδ complex in the presence of neutral (black) and anionic (gray) raft membranes. The shaded bars indicate the data for the PDEδ-complexed K-Ras4B. In addition, the effect of Arl2^{GTP} on the PDEδ binding affinity is shown. The error bars represent the standard deviation from 3–9 measurements. All kinetic parameters are given in Tables S1 and S2 [SI].

rate of K-Ras4B is mirrored in the corresponding dissociation rate, that is, the presence of PDEδ retards the dissociation of K-Ras4B from the anionic and neutral raft membranes to kinetic values comparable to those detected for PDEδ alone (Figure 2c).

In addition, the amount of quasi-irreversibly bound protein is—within the accuracy of the experiments—not changed by complexation of K-Ras4B with PDEδ (Figure S1b [SI]; all kinetic parameters are summarized in Tables S1 and S2 [SI]). This would indicate that active and inactive K-Ras4B are still able to stably insert into membranes and therefore raises the question if K-Ras4B is still bound to PDEδ upon membrane partitioning. Binding of K-Ras4B to PDEδ buries the lipid anchor of K-Ras4B in the hydrophobic binding pocket of PDEδ and is thus expected to inhibit stable insertion of the farnesyl moiety into the membrane. However, the active Arf-like protein 2 (Arl2^{GTP}) decreases the binding affinity of PDEδ to K-Ras4B in bulk solution and hence the SPR data essentially reflect the membrane binding of K-Ras4B GTP by the simultaneous presence of the PDEδ–Arl2^{GTP} complex (Figure 2).

Dynamical Properties of the K-Ras4B and PDEδ Membrane Interaction. Frequency-domain fluorescence anisotropy was used to further characterize the interaction of GDP- and GTP-loaded K-Ras4B with PDEδ and heterogeneous membranes. According to the (rotational) Stokes–Einstein relation, the rotational correlation time, $\theta_{protein}$, determined experimentally is proportional to the size (hydrodynamic volume) of the fluorescent protein, i.e., the BODIPY-labeled K-Ras4B. In aqueous buffer solution, an overall rotational correlation time of around 14 ns is detected for GDP- and GTP-loaded K-Ras4B as well as a truncated K-Ras4B protein (devoid of the farnesyl anchor) that served as control (Figure 3 and Table S4 [SI]). Whereas the control protein

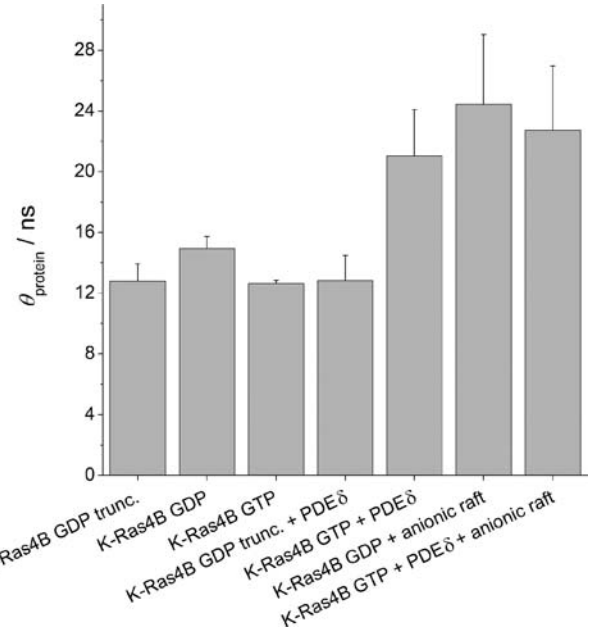

Figure 3. Overall rotational correlation times of BODIPY-labeled K-Ras4B at T = 25 °C. Results are shown for GDP- and GTP-loaded K-Ras4B in the presence and absence of PDEδ and/or heterogeneous model raft membranes. The underlying fitting parameters are given in Tables S3 and S4 [SI].

shows no binding to PDEδ (θ = 12.9 ns), an almost doubling of θ can be observed (θ = 21.1 ns) upon addition of PDEδ to K-Ras4B due to complex formation of the nearly equally sized proteins. The further addition of lipid vesicles composed of the anionic lipid raft mixture to the K-Ras4B/PDEδ complex does not significantly alter the rotational dynamics of K-Ras4B (θ = 22.7 ns). Corroborated by the SPR, IRRAS, and AFM data (see above and below), which all reveal an interaction of the dissociated complex with the membrane, the possibility that the

dx.doi.org/10.1021/ja305518h | J. Am. Chem. Soc. 2012, 134, 11503–11510

K-Ras4B/PDEδ complex stays intact and does not interact with the membrane can be excluded as a reason for the absence of any further changes in θ upon addition of the lipid vesicles. The latter would point toward a dissociation of the K-Ras4B/PDEδ complex upon membrane interaction, since a retardation of the protein rotational dynamics on the order of 10 ns would be expected for an interaction of the intact complex with the anionic membrane (cf. data for K-Ras4B GDP + anionic raft, Figure 3).

Lateral Segregation of K-Ras4B and PDEδ in Heterogeneous Membranes. To further confirm the dissociation of the K-Ras4B/PDEδ complex upon membrane interaction and to gain complementary spatial information on the single molecule level with an imaging technique, time-lapse tapping mode atomic force microscopy (AFM) experiments were carried out. To this end, mica-supported lipid bilayers were prepared and after ensuring the formation of a coherent, defect-free lipid membrane, the protein solution was injected into the AFM fluid cell. The protein−membrane interaction process was followed by imaging the same membrane region at various time points. Figure 4 shows that the anionic raft membrane

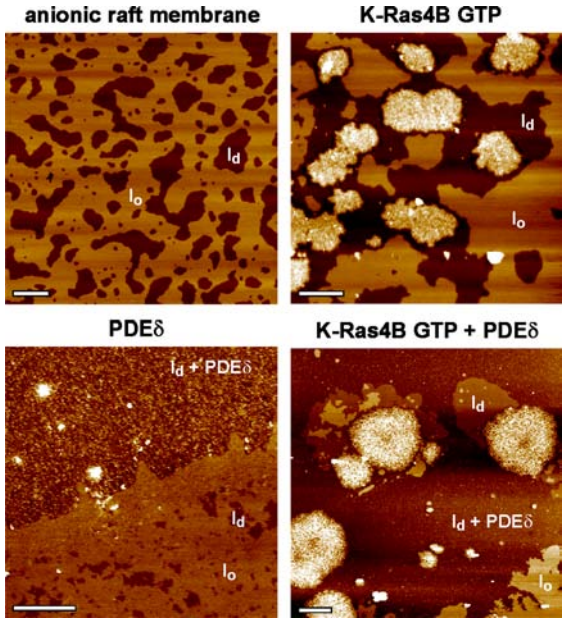

Figure 4. AFM images of the interaction of K-Ras4B GTP, PDEδ, and the preformed K-Ras4B/PDEδ complex with anionic raft membranes. The upper left panel shows a representative AFM image of the anionic raft membrane before injection of 200 μL protein solution ($c_{\text{K-Ras4B}}$ = 2 μM and $c_{\text{PDE}\delta}$ = 3.4 μM) into the AFM fluid cell. The AFM images of K-Ras4B GTP,[13] PDEδ, and K-Ras4B GTP + PDEδ display the membrane partitioning of the proteins at a particular time point, i.e., at $t \approx 21$ h. The overall height of the vertical color scale from dark brown to white corresponds to 6 nm for all images; the scale bar represents 1 μm.

segregates into liquid-ordered (l_o) and liquid-disordered (l_d) domains, which is indicated by a height difference of the two phases of about 1.0 nm.[26,27] Upon partitioning of GTP-loaded K-Ras4B into the membrane, the formation of new K-Ras4B GTP-enriched domains inside a fluid-like environment can be observed, with a mean thickness of the protein clustered domains of 1.8 ± 0.2 nm with respect to the pure l_d phase (Figure 4).[13] In contrast, a homogeneous distribution in the l_d phase of the membrane is detected for PDEδ. At the same time, the partitioning of PDEδ into the membrane leads to a thinning of the fluid l_d phase of about 0.5 nm. The mean height of PDEδ has been determined to be 1.1 ± 0.2 nm. Remarkably, when the K-Ras4B GTP/PDEδ complex, which was preformed in bulk solution, was added to the anionic raft membrane, the AFM images clearly mirror the membrane partitioning behavior of the single components (Figure 4). This means that both, new domains with accumulated K-Ras4B GTP protein (mean thickness 1.6 ± 0.3 nm) and homogeneously distributed PDEδ with a mean height of 1.3 ± 0.5 nm in an ∼0.5 nm thinned l_d phase, are detected. These findings argue for an exposure of the K-Ras4B farnesyl anchor and thus dissociation of the K-Ras4B GTP/PDEδ complex upon membrane interaction. The same scenario was observed for K-Ras4B GTP, PDEδ, and the corresponding complex partitioning into neutral raft membranes, pointing toward an interaction behavior that is independent of the membrane composition (Figure S2 [SI]).

Structure and Orientation of K-Ras4B and PDEδ at Heterogeneous Membranes. Infrared reflection absorption (IRRA) spectroscopy allows following the combined effects of orientational and structural changes of proteins that are adsorbed to or inserted into lipid monolayers (including changes in the strength of interaction).[35] Since our recent transmission Fourier-transform infrared (FTIR) spectroscopy experiments revealed that K-Ras4B does not undergo significant secondary structural changes in the presence of membranes, changes in the position, intensity, and shape of the amide-I′ band in the IRRA spectra can be assigned to changes in the protein orientation upon membrane insertion.[13] By simultaneously recording IRRA spectra and surface pressure/time (π/t) isotherms, the interaction of K-Ras4B and PDEδ with lipid monolayers composed of the anionic raft mixture could be studied and the associated orientational changes examined (Figure 5). The IRRA spectra of the amide-I′ region of K-Ras4B GTP reveal a shift in wavenumber of the band maximum between 1638 and 1647 cm^{-1} within the experimental time frame, suggesting a reorientation of the G-domain of the active protein at the lipid interface during membrane insertion (Figure 5a). This would imply that K-Ras4B GTP exhibits a high orientational flexibility, that is, spans a large set of orientations, resulting in a more randomized orientation of its G-domain with respect to the lipid interface. The corresponding π/t-profile is indicative of an effective insertion of the farnesyl anchor of K-Ras4B into the lipid monolayer, leading to a marked increase in surface pressure with proceeding membrane insertion (Figure 5d). The injection of K-Ras4B underneath the lipid monolayer was accomplished at a surface pressure of about 30 mN/m, which reflects the lipid density generally observed in physiological lipid membranes.

In contrast to K-Ras4B, when adding PDEδ only, the surface pressure profile reveals the absence of significant insertion (Figure 5d). However, PDEδ does seem to interact with the lipid headgroup region as evident by the minor changes in the surface pressure profile with time. This is further supported by the strong amide-I′ band intensity in the IRRA spectra, which is indicative of an adsorption of PDEδ at the lipid interface (Figure 5b). The band maximum at around 1624 cm^{-1} is characteristic for a predominantly antiparallel β-sheet structure, in accordance with the immunoglobulin-like β-sandwich fold determined for PDEδ by crystallography.[17,21] By using p-polarized light in IRRAS, the change in the sign of the amide-I′

dx.doi.org/10.1021/ja305518h | J. Am. Chem. Soc. 2012, 134, 11503−11510

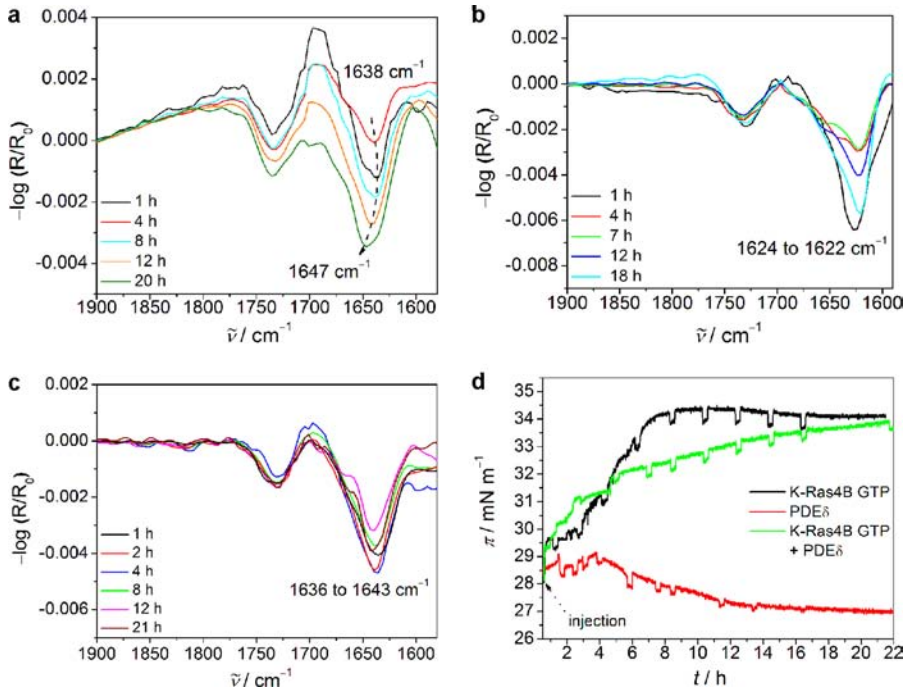

Figure 5. IRRA spectra for (a) K-Ras4B GTP (reproduced from ref 13), (b) PDEδ, and (c) the preformed K-Ras4B GTP/PDEδ complex inserted into or adsorbed at the anionic lipid raft monolayer (kept at ~30 mN m^{-1}) acquired with p-polarized light at an angle of incidence of 35°. Panel d shows the surface pressure profiles for K-Ras4B GTP (black), PDEδ (red), and the preformed K-Ras4B GTP/PDEδ complex (green) upon interaction with the lipid raft monolayer.

band from negative below to positive above the Brewster angle can be assigned to a parallel orientation of the β-sheets of PDEδ to the membrane interface (Figure S4 [SI]).

Finally, measurements were conducted with the K-Ras4B GTP/PDEδ complex preformed in bulk solution. Figure 5d shows that the surface pressure profile resembles that of the active K-Ras4B monolayer interaction, that is, the insertion of K-Ras4B GTP into the lipid monolayer. This finding also supports the assumption that the K-Ras4B GTP/PDEδ complex dissociates upon membrane contact, setting the lipid anchor of K-Ras4B free for stable membrane insertion. In addition, the band maximum shift in the IRRA spectra between 1636 and 1643 cm^{-1} reflects the characteristic band shift of K-Ras4B GTP at the anionic raft membrane, whereas the PDEδ band at 1624 cm^{-1} cannot be detected (Figure 5c). However, the absence of the characteristic IR band for PDEδ does not imply that PDEδ is no longer able to interact with the membrane, but that adsorption at the membrane interface of the less strongly bound PDEδ is possibly partially suppressed by the dominant K-Ras4B−membrane interaction, since an excess of K-Ras4B was used with respect to the surface area of the Langmuir trough. Hence, the contribution of PDEδ to the IRRA intensity seems to be alleviated by the membrane-bound K-Ras4B GTP. The same conclusions can be drawn from comparative experiments performed with GDP-loaded K-Ras4B and PDEδ, pointing toward a membrane interaction process that is independent of nucleotide loading (Figure S3 [SI]).

Analysis of the K-Ras4B and PDEδ Interaction by Intrinsic Fluorescence Spectroscopy. PDEδ contains four tryptophan and two tyrosine residues, with one of each being involved in (Y149) or closely related to (W32) the hydrophobic binding pocket of PDEδ (cf. Figure 1).[21,23] The intrinsic fluorescence of PDEδ is mainly due to the emission of tryptophan, with some contribution from tyrosine. While monitoring the emission spectra of PDEδ in the absence and presence of K-Ras4B GTP (that has nine tyrosines but no tryptophan) and the anionic raft membrane, changes in the band maximum and shape can be related to structural changes in the environment of the fluorophor (Figure 6). The

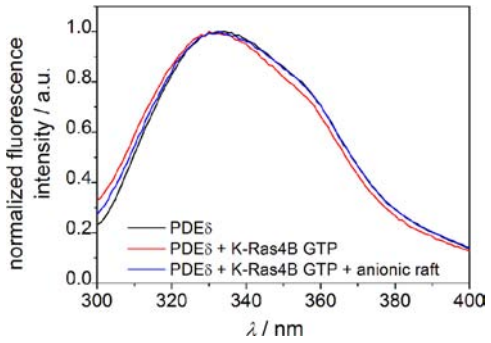

Figure 6. Normalized fluorescence spectra of PDEδ in bulk solution (black), the K-Ras4B GTP/PDEδ complex in bulk solution (red), and the K-Ras4B GTP/PDEδ complex upon interaction with the anionic raft membrane (blue) at 25 °C. The spectra show the change of the PDEδ tryptophan emission maximum and band shape upon complexation and membrane-mediated dissociation of the PDEδ and K-Ras4B GTP complex.

asymmetric emission band reflects the different locations of the fluorescent residues in PDEδ, that is, fluorescent residues that are buried in nonpolar regions of the protein as well as residues that are located at the protein surface and thus exposed to the aqueous solution. When K-Ras4B binds to PDEδ by insertion of its lipid farnesyl anchor into the hydrophobic binding pocket of PDEδ, a blue shift to lower wavelengths is observed in the fluorescence spectra, which is indicative for a

dx.doi.org/10.1021/ja305518h | J. Am. Chem. Soc. 2012, 134, 11503−11510

decrease in the polarity of the fluorophor's surroundings. This shift turned out to be reversible and the initial fluorescence spectrum of PDEδ was recovered when lipid vesicles composed of the anionic raft mixture were added to the K-Ras4B GTP/PDEδ complex, arguing for a dissociation of the farnesyl from the binding pocket of PDEδ (Figure 6). The same behavior was observed for the interaction of PDEδ with GDP-loaded K-Ras4B in the presence of anionic membranes (Figure S5a [SI]), pointing toward a nucleotide-independent process. Conversely, when the experiment was carried out with an unlipidated K-Ras4B protein, no blue shift of the PDEδ fluorescence spectrum could be detected (Figure S5b [SI]). Owing to the fact that K-Ras4B GTP and PDEδ show the same partitioning behavior in neutral raft membranes and that the effect of PDEδ on the membrane interaction of K-Ras4B has been demonstrated to be independent of the membrane composition, a similar behavior is expected in the tryptophan assay with the neutral raft mixture.

To additionally confirm the dissociation of the K-Ras4B/PDEδ complex upon membrane interaction, a FRET-based assay was carried out, using the tryptophan of PDEδ as donor and a dansyl-labeled K-Ras4B as acceptor. The marked FRET-induced change in the donor emission demonstrates the binding of PDEδ to K-Ras4B in solution by quenching of the intrinsic Trp fluorescence. In turn, as expected, the dissociation of the complex upon addition of anionic lipid raft vesicles is indicated by an increase in the intrinsic Trp fluorescence (Figure S6 [SI]).

DISCUSSION AND CONCLUSION

Recently, prenyl-binding proteins such as PDEδ came into focus as potential targets for Ras inhibitors and anticancer drugs, providing another possibility to block Ras signaling pathways and stop the oncogenic activity of Ras.[36] In a previous study of our group, the interaction of K-Ras4B with anionic and neutral lipid raft membranes has been investigated and K-Ras4B was shown to form protein-enriched microdomains, probably acting as effective signaling platforms.[13] The molecular mechanism of PDEδ-mediated changes in K-Ras4B membrane association remained elusive up to now. Our SPR data show unambiguously that K-Ras4B remains stably anchored in lipid membranes upon addition of PDEδ to membrane-bound K-Ras4B, independent of GDP/GTP-loading and membrane composition, thus contradicting the proposed membrane-extracting function of PDEδ.[18,22] This finding can be rationalized recalling the binding of PDEδ to K-Ras4B, which occurs mainly through the farnesylated C-terminus of K-Ras4B and is thought to be triggered by the negatively charged surface of PDEδ in the vicinity of the positively charged K-Ras4B C-terminus.[21] When the lipid anchor of membrane-bound K-Ras4B is stably inserted into the lipid membrane (supported by strong electrostatic interactions of the Lys stretch in the HVR of K-Ras4B with the anionic lipid interface), there is no exposed binding site available for PDEδ, since it has been shown that there exist no additional contact sites between PDEδ and the Ras G-domain.[21] Also, given that the binding affinity of PDEδ to farnesylated K-Ras4B (K_D = 0.3 μM)[20] is of similar order of magnitude as the K-Ras4B membrane binding affinity ($K_D \approx 2-20$ μM), membrane extraction of K-Ras4B does not seem to be favorable. In addition, PDEδ itself exhibits a relatively strong affinity to heterogeneous membranes ($K_D \approx$ 0.3 μM, Tables S1 and S2 in SI).

Interestingly, when the K-Ras4B/PDEδ complex preformed in bulk solution is exposed to heterogeneous membranes, a release of farnesylated K-Ras4B can be observed. As concluded from all spectroscopic and microscopic data obtained, the exposure of the K-Ras4B/PDEδ complex to the lipid membrane led to a situation that reflected the membrane partitioning behavior of the single components, i.e., homogeneously distributed PDEδ was found along with K-Ras4B-enriched protein domains. Moreover, the membrane interaction behavior with PDEδ has been shown to be independent of K-Ras4B nucleotide loading, in agreement with literature *in vivo* data.[17,18,21] Finally, SPR revealed an enhanced membrane affinity of the K-Ras4B/PDEδ complex, particularly in the presence of negatively charged membranes ($K_D \approx 61-87$ nM). Hence, PDEδ seems to function as a solubilizing factor for K-Ras4B in the cytosol, and effectively delivers farnesylated K-Ras4B to the plasma membrane. This probably occurs by an increase in the cytoplasmic diffusion and thereby enhancement of the kinetics of electrostatic trapping at the negatively charged plasma membrane, as shown lately.[25] Upon contact of the PDEδ-complexed K-Ras4B with the plasma membrane, a dissociation of the complex takes place that leads to an exposure of the once shielded K-Ras4B's membrane anchor and thus insertion of the farnesyl residue into the plasma membrane, resulting in K-Ras4B-enriched microdomain formation and finally signaling.[13] From the AFM experiments it can also be revealed that PDEδ binds to the membrane after dissociation of the complex. While the lateral segregation and associated membrane microdomain formation of K-Ras4B and PDEδ were shown to be independent of the membrane composition, the membrane interaction kinetics and thus membrane binding affinities were demonstrated to be influenced by the presence of anionic lipids in the membrane.

The release of K-Ras4B from the plasma membrane is thought to occur through phosphorylation at serine 181.[37] SPR measurements of our group support this idea by revealing a reduced affinity of phosphorylated K-Ras4B to homogeneous anionic membranes. Thereby, the initial slope of the sensorgram for the binding of phosphorylated K-Ras4B to a membrane composed of POPC/POPS with a molar ratio of 8:2 is reduced about 2-fold with respect to the unphosphorylated K-Ras4B GDP (34.6 $\pm$ 15.2 RU s^{-1} and 15.5 $\pm$ 1.8 RU s^{-1} for K-Ras4B GDP and phospho-K-Ras4B GDP, respectively). Furthermore, $Arl2^{GTP}$ has been shown to actively displace farnesylated Rheb from PDEδ[21] and also seems to decrease the binding affinity of PDEδ to K-Ras4B, as suggested by our SPR data. To conclude, our results are in accordance with recent *in vivo* studies, revealing that PDEδ sustains the spatial organization of K-Ras4B in cells by enriching K-Ras4B at the plasma membrane for augmented signaling owing to facilitated diffusion of the PDEδ-solubilized K-Ras4B in the cytoplasm.[25]

MATERIALS AND METHODS

Materials. The phospholipids 1,2-dioleoyl-*sn*-glycero-3-phosphocholine (DOPC), 1,2-dioleoyl-*sn*-glycero-3-phospho-(1′-*rac*-glycerol) sodium salt (DOPG), 1,2-dipalmitoyl-sn-glycero-3-phospho-(1′-rac-glycerol) sodium salt (DPPG), and 1,2-dipalmitoyl-*sn*-glycero-3-phosphocholine (DPPC) were purchased from Avanti Polar Lipids (Alabaster, USA). Cholesterol (Chol) and 4-(2-hydroxyethyl)-piperazine-1-ethanesulfonic acid (Hepes) were from Sigma Aldrich (Deisenhofen, Germany). Magnesium chloride, tris(hydroxymethyl)-aminomethan (Tris), and chloroform were obtained from Merck (Darmstadt, Germany). The fluorescent lipid *N*-(lissamine rhodamine

B sulfonyl)-1,2-dihexadecanoyl-*sn*-glycero-3-phosphoethanolamine triethylammonium salt (*N*-Rh-DHPE) and BODIPY-FL were from Molecular Probes (Invitrogen).

Protein Synthesis. The synthesis of the K-Ras4B proteins is described in detail in ref 20. Briefly, the *S*-farnesylated K-Ras4B protein was synthesized by a combination of expressed protein ligation (EPL) and lipopeptide synthesis. Details on the nucleotide exchange and BODIPY-labeling of K-Ras4B proteins are available in ref 13 and the SI. $Arl2^{GTP}$ (GppNHp-bound state as a nonhydrolyzable GTP analogue) and His6-tagged PDEδ were expressed as described previously.[23,38]

Surface Plasmon Resonance (SPR). SPR experiments were carried out with a Biacore 3000 system (Biacore, Uppsala, Sweden; now GE Healthcare). For the protein−membrane interaction studies, the pioneer L1 sensor chip (GE Healthcare, Munich, Germany) was used. Details of sample preparation, vesicle immobilization, performance of SPR measurements, regeneration of the chip surface, and analysis of the SPR sensorgrams have been described before[32] and are given in the SI. For the curve-fitting procedure, the BIAevaluation software 4.1 (Biacore, Uppsala, Sweden) and Origin 7 (OriginLab Corporation, Northampton, MA) were used.

Atomic Force Microscopy (AFM). The preparation of the supported lipid bilayers and the AFM setup is described in detail in refs 13 and 33 and the SI. For the protein−membrane interaction studies, 200 μL of either K-Ras4B (2 μM), PDEδ (3.4 μM), or K-Ras4B GTP/PDEδ (2 μM/3.4 μM) in 20 mM Tris, 7 mM $MgCl_2$, pH 7.4 were injected into the AFM fluid cell at room temperature and allowed to incubate for 1 h. Measurements were performed on a MultiMode scanning probe microscope equipped with a NanoScope IIIa controller (Digital Instruments, Santa Barbara, CA) and a J-Scanner (scan size 125 μm). Images were obtained by applying the tapping mode in liquid with sharp nitride lever (SNL) probes mounted in a fluid cell (MTFML, Veeco, Mannheim, Germany).

Infrared Reflection Absorption Spectroscopy (IRRAS). The experiments were carried out on an IRRAS setup consisting of two linked Teflon troughs and a Vertex 70 FT-IR spectrometer connected to an A511 reflection attachment (both Bruker, Germany) with an MCT detector. Details on the setup, sample preparation, and spectra analysis are given in ref 13 and the SI.

Fluorescence Anisotropy and Spectroscopy. All fluorescence spectroscopy measurements were performed on a K2 multifrequency phase and modulation fluorometer (ISS Inc., Champaign, IL). BODIPY-labeled K-Ras4B was excited by use of a 473 nm laser diode directly connected to a function generator, yielding modulated excitation light over a frequency range of 2−173 MHz at a cross-correlation frequency of 400 Hz. The BODIPY-emission was collected through a 505 nm long-pass filter. Fluorescence lifetime measurements were carried out at magic-angle conditions prior to the anisotropy experiments. Experimental data were fitted with the VINCI-Analysis software (ISS Inc., Champaign, IL) to yield fluorescence lifetimes and rotational correlation times. The tryptophan emission spectrum of 6.8 μM PDEδ in Tris buffer (excitation at 282 nm) was collected upon addition of K-Ras4B GTP (4 μM) and finally after the addition of anionic raft vesicles. A more detailed description of the setup, sample preparation, and data analysis can be found in the SI.

■ ASSOCIATED CONTENT

Supporting Information

Details on materials and sample preparation as well as protein synthesis. Further information on the conduction of the SPR experiments including sample preparation, vesicle immobilization, performance of the SPR measurements, regeneration of the chip surface, and analysis of the SPR sensorgrams. Details on the performance of IRRAS, AFM, and fluorescence anisotropy and spectroscopy measurements. Figures S1−S6 and Tables S1−S4 as described in the text. This material is available free of charge via the Internet at http://pubs.acs.org.

■ AUTHOR INFORMATION

Corresponding Author

roland.winter@tu-dortmund.de

Notes

The authors declare no competing financial interest.

■ ACKNOWLEDGMENTS

This research was supported by the Deutsche Forschungsgemeinschaft (DFG SFB 642) and the Max Planck Society (IMPRS Chemical Biology). We are grateful to Christine Nowak for technical assistance and to Dr. Shehab A. Ismail and Prof. Alfred Wittinghofer from the Max Planck Institute of Molecular Physiology in Dortmund for providing us with $Arl2^{GTP}$.

■ REFERENCES

(1) Mitsuuchi, Y.; Testa, J. R. *Am. J. Med. Genet.* **2002**, *115*, 183−188.
(2) Grady, W. M.; Markowitz, S. D. *Annu. Rev. Genomics Hum. Genet.* **2002**, *3*, 101−128.
(3) Jaffee, E. M.; Hruban, R. H.; Canto, M.; Kern, S. E. *Cancer Cell* **2002**, *2*, 25−28.
(4) Wittinghofer, A.; Waldmann, H. *Angew. Chem., Int. Ed.* **2000**, *39*, 4192−4214.
(5) Hancock, J. F. *Nat. Rev. Mol. Cell Biol.* **2003**, *4*, 373−384.
(6) Wittinghofer, A.; Pal, E. F. *Trends Biochem. Sci.* **1991**, *16*, 382−387.
(7) Hancock, J. F.; Paterson, H.; Marshall, C. J. *Cell* **1990**, *63*, 133−139.
(8) Jackson, J. H.; Li, J. W.; Buss, J. E.; Der, C. J.; Cochrane, C. G. *Proc. Natl. Acad. Sci. U.S.A.* **1994**, *91*, 12730−12734.
(9) Marshall, C. J. *Curr. Opin. Cell. Biol.* **1996**, *8*, 197−204.
(10) Willumsen, B. M.; Christensen, A.; Hubbert, N. L.; Papageorge, A. G.; Lowy, D. R. *Nature* **1984**, *310*, 583−586.
(11) Gomez, G. A.; Daniotti, J. L. *FEBS J.* **2007**, *274*, 2210−2228.
(12) Leventis, R.; Silvius, J. R. *Biochemistry* **1998**, *37*, 7640−7648.
(13) Weise, K.; Kapoor, S.; Denter, C.; Nikolaus, J.; Opitz, N.; Koch, S.; Triola, G.; Herrmann, A.; Waldmann, H.; Winter, R. *J. Am. Chem. Soc.* **2011**, *133*, 880−887.
(14) Vartak, N.; Bastiaens, P. *EMBO J.* **2010**, *29*, 2689−2699.
(15) Apolloni, A.; Prior, I. A.; Lindsay, M.; Parton, R. G.; Hancock, J. F. *Mol. Cell. Biol.* **2000**, *20*, 2475−2487.
(16) Choy, E.; Chiu, V. K.; Silletti, J.; Feoktistov, M.; Morimoto, T.; Michaelson, D.; Ivanov, I. E.; Philips, M. R. *Cell* **1999**, *98*, 69−80.
(17) Hanzal-Bayer, M.; Renault, L.; Roversi, P.; Wittinghofer, A.; Hillig, R. C. *EMBO J.* **2002**, *21*, 2095−2106.
(18) Nancy, V.; Callebaut, I.; El Marjou, A.; de Gunzburg, J. *J. Biol. Chem.* **2002**, *277*, 15076−15084.
(19) Zhang, H.; Liu, X. H.; Zhang, K.; Chen, C. K.; Frederick, J. M.; Prestwich, G. D.; Baehr, W. *J. Biol. Chem.* **2004**, *279*, 407−413.
(20) Chen, Y. X.; Koch, S.; Uhlenbrock, K.; Weise, K.; Das, D.; Gremer, L.; Brunsveld, L.; Wittinghofer, A.; Winter, R.; Triola, G.; Waldmann, H. *Angew. Chem., Int. Ed.* **2010**, *49*, 6090−6095.
(21) Ismail, S. A.; Chen, Y. X.; Rusinova, A.; Chandra, A.; Bierbaum, M.; Gremer, L.; Triola, G.; Waldmann, H.; Bastiaens, P. I.; Wittinghofer, A. *Nat. Chem. Biol.* **2011**, *7*, 942−949.
(22) Bhagatji, P.; Leventis, R.; Rich, R.; Lin, C. J.; Silvius, J. R. *Biophys. J.* **2010**, *99*, 3327−3335.
(23) Alexander, M.; Gerauer, M.; Pechlivanis, M.; Popkirova, B.; Dvorsky, R.; Brunsveld, L.; Waldmann, H.; Kuhlmann, J. *ChemBioChem* **2009**, *10*, 98−108.
(24) Marzesco, A. M.; Galli, T.; Louvard, D.; Zahraoui, A. *J. Biol. Chem.* **1998**, *273*, 22340−22345.
(25) Chandra, A.; Grecco, H. E.; Pisupati, V.; Perera, D.; Cassidy, L.; Skoulidis, F.; Ismail, S. A.; Hedberg, C.; Hanzal-Bayer, M.; Venkitaraman, A. R.; Wittinghofer, A.; Bastiaens, P. I. *Nat. Cell Biol.* **2012**, *14*, 148−158.

(26) Kapoor, S.; Werkmüller, A.; Denter, C.; Zhai, Y.; Markgraf, J.; Weise, K.; Opitz, N.; Winter, R. *Biochim. Biophys. Acta* **2011**, *1808*, 1187−95.
(27) Evers, F.; Jeworrek, C.; Weise, K.; Tolan, M.; Winter, R. *Soft Matter* **2012**, *8*, 2170−2175.
(28) Green, R. J.; Frazier, R. A.; Shakesheff, K. M.; Davies, M. C.; Roberts, C. J.; Tendler, S. J. *Biomaterials* **2000**, *21*, 1823−1835.
(29) Mozsolits, H.; Thomas, W. G.; Aguilar, M. I. *J. Pept. Sci.* **2003**, *9*, 77−89.
(30) Besenicar, M.; Macek, P.; Lakey, J. H.; Anderluh, G. *Chem. Phys. Lipids* **2006**, *141*, 169−178.
(31) Cooper, M. A.; Hansson, A.; Löfås, S.; Williams, D. H. *Anal. Biochem.* **2000**, *277*, 196−205.
(32) Gohlke, A.; Triola, G.; Waldmann, H.; Winter, R. *Biophys. J.* **2010**, *98*, 2226−2235.
(33) Weise, K.; Triola, G.; Brunsveld, L.; Waldmann, H.; Winter, R. *J. Am. Chem. Soc.* **2009**, *131*, 1557−1564.
(34) Vogel, A.; Reuther, G.; Weise, K.; Triola, G.; Nikolaus, J.; Tan, K. T.; Nowak, C.; Herrmann, A.; Waldmann, H.; Winter, R.; Huster, D. *Angew. Chem., Int. Ed.* **2010**, *48*, 8784−8787.
(35) Mendelsohn, R.; Mao, G.; Flach, C. R. *Biochim. Biophys. Acta* **2010**, *1798*, 788−800.
(36) Kloog, Y.; Cox, A. D. *Semin. Cancer Biol.* **2004**, *14*, 253−261.
(37) Bivona, T. G.; Quatela, S. E.; Bodemann, B. O.; Ahearn, I. M.; Soskis, M. J.; Mor, A.; Miura, J.; Wiener, H. H.; Wright, L.; Saba, S. G.; Yim, D.; Fein, A.; Pérez de Castro, I.; Li, C.; Thompson, C. B.; Cox, A. D.; Philips, M. R. *Mol. Cell* **2006**, *21*, 481−493.
(38) Kühnel, K.; Veltel, S.; Schlichting, I.; Wittinghofer, A. *Structure* **2006**, *14*, 367−378.